Implementation of a 2D Panel Method for Potential Flow Past Multi-Element Airfoil Configurations

Diogo Matos Chaves, Nr. 57116
Student of Master in Mechanical Engineering
Instituto Superior Técnico, Technical University of Lisbon

An implementation in MATLAB of a 2D panel method was performed for use in applications with airfoils in ground effect and multi-element configurations. The code was based on an earlier code developed in the FORTRAN language, using a 1st order panel method that followed an implementation with constant source and vortex strengths and flat panels. The description of the method used is included, as is the methodology used in the development of the code. An extensive verification procedure to quantify the uncertainty and the error convergence was performed both for single airfoils and for multi-element configurations. Also, several examples of possible applications of the program were analyzed, where the results obtained with the developed code were compared with some experimental and CFD results available in relevant papers. Regarding profiles in ground effect, it is demonstrated that the trends of the lift coefficient and pressure distribution results follow those of the experimental or CFD results, making this code an ideal tool for qualitative analyses and optimization of geometries and relative orientations between airfoils.

Keywords: Panel Methods, Multi-Element, Ground Effect, High-Lift Devices

Nomenclature

C_{L_Γ} – Lift coefficient from circulation
C_L – Lift coefficient from pressure integration
C_D – Drag coefficient from pressure integration
C_P – Pressure coefficient
α – Angle of attack
c – Chord length of the airfoil
2D – Two dimensional
3D – Tri dimensional
CFD – Computational fluid dynamics
V_∞ – Free-stream velocity
u, v – Velocity components in x and y axis system
$u_{s_{ij}}$, $v_{s_{ij}}$ – Influence of panel j in panel i due to a source
$u_{v_{ij}}$, $v_{v_{ij}}$ – Influence of panel j in panel i due to a vortex
ϕ_∞ – Uniform flow
θ_i – Angle of panel i with respect the x axis
N – Number of panels in an airfoil
q_j – Source strength in panel j
γ_o – Constant vortex strength
s_{m_i} – Length of mean line panel i
γ – Corrected vortex strength
Γ – Total circulation around an airfoil
b_i – Vector relating to the uniform flow
A_{ij} – Normal influence coefficients matrix
B_{ij} – Tangential influence coefficients matrix
C_{ij} – Matrix containing individual A_{ij} matrices
Q_i – Vector containing each body singularities
B_i – Vector containing each individual b_i vectors
D_{ij} – Matrix containing individual B_{ij} matrices
T_i – Tangential velocities due to singularities
l_{m_i} – Length of surface panel i
x_{bp_i} – x coordinate of border point i
y_{bp_i} – y coordinate of border point i
C_x – Pressure integration in the x direction
C_y – Pressure integration in the y direction
LE – Leading edge
TE – Trailing edge
U_{mn}, V_{mn} – Influence Coefficients on point m in the x and y axis due to a singularity n
h/c – Distance to the wall parameterized by the chord
e_o – Error for zero panel size
$\frac{h_i}{h_1}$ – Grid refinement ratio
p – Observed Order of accuracy
β – Constant
e_{ϕ_i} – Numerical error of parameter ϕ_i

Introduction

The first 2D implementations of potential flow calculations made possible by computers were the so called *Panel Methods*, which were first developed by Hess & Smith in the 60's decade of the last century. These methods allowed the calculation of flows past complex arbitrary shapes by discretizing the body's surface in several segments (panels), distributing singularities in those segments and then solving the Laplace's equation as a sum of all the singularity contributions in each panel. These methods have the advantage of being able to be applied to virtually all kinds of geometries and also of handling more than one body in the same problem. Furthermore, when calculations are made at small angles of attack, there's a great correlation with experimental results.

When the first computers capable of handling potential flow calculations appeared, the 2D calculations were the ones that first received attention, with many commercial and non-commercial codes developed during this time, including implementations of panel methods. As computers calculation capabilities progressed, there was a trend towards the development of codes that could handle

3D geometries or viscous flow, not only because of their more stimulating nature, but also because of their undoubtedly increased prediction capability of the real flows. As such, inviscid 2D codes began to lose importance and development effort focus to more complex codes, having been put aside as not an option for most calculations. However, although 3D panel methods and CFD codes are more exciting because of their more exact nature, there is scarcely any situation that couldn't benefit from a previous 2D analysis [1], not only for the easiness of use of these codes, but also because of their good numerical precision with a relatively small system of equations and their calculation time being only a fraction of that of more complex codes. As such, even though nowadays most calculations are made with CFD codes, there are some calculations that are best made with this kind of methods. In situations where the most important is the speed and the qualitative results, the 2D panel methods can be of great advantage. Sun, S. used a 2nd order panel method in order to optimize the front wing of a Formula One car [2], while Wickramasinghe, U. et al. also used a similar code to investigate the best geometry for an airfoil [3]. Though not as recent as the optimizations cited above, Katz, J. [4] [5] [6] [7] and Knowles, K. [8] also used 2D panel methods to investigate airfoils in ground effect.

Hence, given the advantages of these kind of methods and their applicability nowadays, the work done was to take a 2D single-element panel method code written in FORTRAN called ASA 2D [9], write it down in MATLAB and then extend the code so that it could handle multi-element calculations. The main goal was to provide an easy to use, fast and reliable code that could be applied in diverse Ground Effect and High-Lift configurations. The method was based in that of Hess & Smith [10], where flat panels and constant singularity strengths were used. The singularities used were sources and sinks to define the geometry of the bodies and vortices applied on the mean line of the bodies to guarantee the satisfaction of the Kutta condition at the trailing edges.

An extensive verification procedure was performed, both for single-element applications, where exact conformal mapping solutions were used to find the absolute error, and also for multi-element configurations, where the goal was to find the relative uncertainty in ground effect situations.

Finally, several ground effect and multi-element situations were thoroughly analyzed, where the results obtained with the developed code were compared with experimental and CFD results available from the literature to find out what the program can and cannot do, and, where applicable, to show the good correlation between experimental or CFD results and those obtained with the code.

Governing Equations

Based on the descriptions from Katz, J. [11], Mason, B. [12] and Moran, J. [13], the equation that governs 2D panel methods for the potential outside an arbitrary body is:

$$\phi(p') = \phi_\infty + \frac{1}{2\pi}\oint_{S_B}\left[q\,ln\,r - \mu\frac{\partial}{\partial n}ln\,r\right]dS \qquad (1\text{ - }1)$$

Although equation **(1 - 1)** states that a body can be approximated through sources and doublets, in the current method only sources are used. As satisfying the Kutta condition is also needed, constant strength vortices are also used, and hence, the potential becomes:

$$\phi = \phi_\infty + \int_{S_B}\frac{q}{2\pi}ln\,r\;dS + \int_{S_B}-\frac{\gamma}{2\pi}\theta\;dS \qquad (1\text{ - }2)$$

After discretization of the surface of the bodies, equation **(1 - 2)** becomes:

$$\phi = \phi_\infty + \sum_{j=1}^{N}\int_{panel\ j}\left[\frac{q(s)}{2\pi}\ln r - \frac{\gamma}{2\pi}\theta\right]dS \qquad (1\text{ - }3)$$

The conditions that need to be satisfied to solve the problem are the zero normal velocity at the surface of each airfoil and the Kutta condition [14] at the trailing edge, both given by the expressions:

$$-u_i\,\mathrm{sen}\,\theta_i + v_i\cos\theta_i = 0 \qquad i = 1,\dots,N \qquad (1\text{ - }4)$$

$$u_1\cos\theta_i + v_1\sin\theta_1 = -u_N\cos\theta_N - v_N\sin\theta_N \qquad (1\text{ - }5)$$

u_i and v_i are respectively the velocities along the x and y axis, given by the equations:

$$u_i = V_\infty\cos\alpha + \sum_{j=1}^{N}q_j u_{s_{ij}} + \gamma\sum_{j=1}^{N}u_{v_{ij}} \qquad (1\text{ - }6)$$

$$v_i = V_\infty\sin\alpha + \sum_{j=1}^{N}q_j v_{s_{ij}} + \gamma\sum_{j=1}^{N}v_{v_{ij}} \qquad (1\text{ - }7)$$

Reorganizing equations **(1 - 4)** and **(1 - 5)** with q_j and γ equaling 1, the following sistem of linear equations is achieved:

$$\begin{bmatrix} A_{1,1} & A_{1,2} & \cdots & A_{1,N} & A_{1,N+1} \\ A_{2,1} & \ddots & & & A_{2,N+1} \\ \vdots & & \ddots & & \vdots \\ A_{N,1} & & & \ddots & A_{N,N+1} \\ A_{N+1,1} & A_{N+1,2} & \cdots & A_{N+1,N} & A_{N+1,N+1} \end{bmatrix}\begin{bmatrix} q_1 \\ q_2 \\ \vdots \\ q_N \\ \gamma \end{bmatrix} = \begin{bmatrix} b_1 \\ b_2 \\ \vdots \\ b_N \\ b_{N+1} \end{bmatrix} \qquad (1\text{ - }8)$$

In equation **(1 - 8)**, each entrance in matrix A_{ij} from line and column 1 to N denotes the influence coefficients due to sources, column $N+1$ denotes the influence coefficients due to vortices and line $N+1$ is the Kutta condition. Vector b_i relates to the uniform flow. After the singularities are known, it is possible to calculate the velocity in each panel through the equation:

$$\begin{gathered} u_{t_i} = u_i\cos\theta_i + v_i\sin\theta_i \\ u_{t_i} = V_\infty(\cos\alpha\cos\theta_i + \sin\alpha\sin\theta_i) + B_{i_j}q_j + B_{i,N+1}\gamma \end{gathered} \qquad (1\text{ - }9)$$

Equation **(1 - 8)** and **(1 - 9)** are the equations for a single body. When there is more than one body, equation **(1 - 10)** applies:

$$C_{ij}Q_i = B_i$$

$$\begin{bmatrix} C_{1,1} & C_{1,2} & \cdots & C_{1,n-1} & C_{1,n} \\ C_{2,1} & \ddots & & & C_{2,n} \\ \vdots & & \ddots & & \vdots \\ C_{n-1,1} & & & \ddots & C_{n-1,n} \\ C_{n,1} & C_{n,2} & \cdots & C_{n,n-1} & C_{n,n} \end{bmatrix}\begin{bmatrix} Q_1 \\ Q_2 \\ \vdots \\ Q_{n-1} \\ Q_n \end{bmatrix} = \begin{bmatrix} B_1 \\ B_2 \\ \vdots \\ B_{n-1} \\ B_n \end{bmatrix} \qquad (1\text{ - }10)$$

Each entrance in matrix C_{ij} denotes an individual matrix A_{ij} defined earlier, which contains the influence coefficients of the panels of a body on the panels of another. $C_{1,2}$ would be for example the influence of body 2

in body 1. Vector B_i should not be confused with matrix B_{ij}. After vector Q_i is known, vector T_i is calculated through the expression **(1 - 11)**:

$$T_i = \begin{bmatrix} D_{1,1} & D_{1,2} & \cdots & D_{1,n-1} & D_{1,n} \\ D_{2,1} & \ddots & & & D_{2,n} \\ \vdots & & \ddots & & \vdots \\ D_{n-1,1} & & & \ddots & D_{n-1,n} \\ D_{n,1} & D_{n,2} & \cdots & D_{n,n-1} & D_{n,n} \end{bmatrix} \begin{bmatrix} Q_1 \\ Q_2 \\ \vdots \\ Q_{n-1} \\ Q_n \end{bmatrix} \quad (1 - 11)$$

Each entrance in matrix D_{ij} denotes an individual matrix B_{ij} that relates to the tangential influence coefficients of a given body on another. Finally, equation **(1 - 12)** is used to calculate the tangential velocity on every panel.

$$u_{t_i} = V_\infty(\cos\alpha\cos\theta_i + \sin\alpha\sin\theta_i) + T_i \quad (1 - 12)$$

And the pressure coefficient through the equation:

$$C_{P_i} = 1 - \left(\frac{u_{t_i}}{V_\infty}\right)^2 \quad (1 - 13)$$

Dimensionless Coefficients

In this method, the vortices are applied in the mean line of the bodies, and as such, according to [9], the vortex strength is given by the equation:

$$\gamma = \gamma_o s_{m_i}^{0.4} \quad (1 - 14)$$

To calculate the lift coefficient through the circulation around the body, the circulation is needed:

$$\Gamma = \int_0^{L_m} \gamma\, ds = \gamma_o \sum_{i=1}^{m} s_{m_i}^{0.4}\, l_{m_i} \quad (1 - 15)$$

In equation **(1 - 15)** m is the number of panels in a body. Finally, the lift coefficient is given by the Kutta-Joukowski equation [14]:

$$C_{L_\Gamma} = \frac{-2\Gamma}{U_\infty c} \quad (1 - 16)$$

It is also possible to calculate the lift coefficient through integration. The lift and drag forces are respectively the perpendicular and parallel components of the aerodynamic force with relation to the free-stream, as is illustrated in Figure 1.

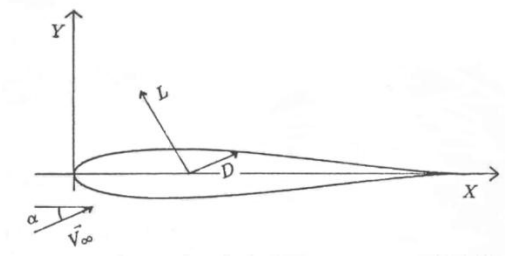

Figure 1 - Aerodynamic Forces

Hence, the lift and drag coefficients are given by the expressions:

$$C_L = C_y\cos\alpha - C_x\sin\alpha \quad (1 - 17)$$

$$C_D = C_x\cos\alpha + C_y\sin\alpha \quad (1 - 18)$$

With C_x and C_y being the middle point integration [15] of the pressure in the x and y directions respectively, given by:

$$C_x = \oint C_p d\left(\frac{y}{c}\right) \cong \sum_{i=1}^{N} C_{p_i}\left(\frac{y_{bp_{i+1}} - y_{bp_i}}{c}\right) \quad (1 - 19)$$

$$C_y = -\oint C_p d\left(\frac{x}{c}\right) \cong -\sum_{i=1}^{N} C_{p_i}\left(\frac{x_{bp_{i+1}} - x_{bp_i}}{c}\right) \quad (1 - 20)$$

Code Organization

The code was separated in 3 parts, namely a pre-processer, a processer and a post-processer.

Pre-Processor

This section of the code is where one defines the geometries of the airfoils and their relative positions. One can decide between generating a 4th series NACA [14], a Joukowski or Karman-Trefftz airfoil [14] or by introducing a file with the points that define a given airfoil.

In order to generate more panels near the leading and trailing edges, the cosine spacing function is used, given by:

$$\frac{x_i}{c} = \frac{1}{2}\left[1 - \cos\left\{\frac{(i-1)\pi}{(N-1)}\right\}\right] \qquad i = 1, \ldots, N \quad (1 - 21)$$

There are two systems of coordinates, one local and another global. The local axis is denoted by x^* and y^* and it is where the coordinates of an airfoil are defined with respect to an origin located on the leading edge, as can be seen in Figure 2. Thus, the x^* axis varies between 0 and 1 (or 0 and 100%), which is the cord length.

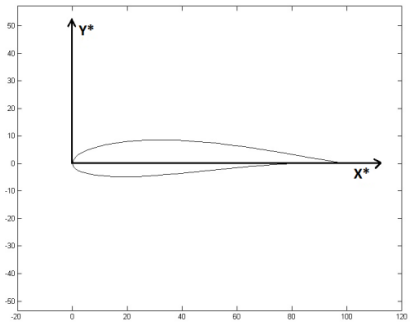

Figure 2 - Local coordinate system

On the other hand, the global axis is denoted by x and y and is where all airfoils are defined with respect to each other with the origin defined arbitrarily, as can be seen in Figure 3.

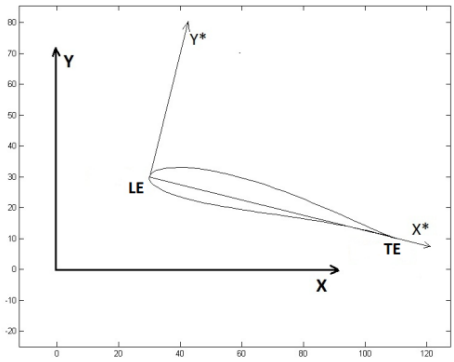

Figure 3 - Global coordinate system

To go from a local axis to the global axis, one needs to perform a rotation, a resizing and a translation according to the defined coordinates of the leading (LE) and trailing (TE) edges. This process starts with finding the angle an airfoil makes with the x axis of the global coordinates, given by:

$$\theta = \tan^{-1}\left(\frac{y_{LE} - y_{TE}}{x_{LE} - x_{TE}}\right) \quad (1 - 22)$$

Knowing the angle of each airfoil, a rotation can be performed based on the equations:

$$x_i = x_i^* \cos\theta - y_i^* \sin\theta \quad (1 - 23)$$

$$y_i = x_i^* \sin\theta + y_i^* \cos\theta \quad (1 - 24)$$

The airfoil size needs to be readjusted with respect to the LE and TE defined. Thus, equation **(1 - 25)** is used to calculate the chord size:

$$chord = \sqrt{(x_{LE} - x_{TE})^2 + (y_{LE} - y_{TE})^2} \quad (1 - 25)$$

Based on the chord of the airfoil, the coordinates can be resized based on the following equations:

$$x_i = x_i^* * \left(\frac{chord}{100}\right) \quad (1 - 26)$$

$$y_i = y_i^* * \left(\frac{chord}{100}\right) \quad (1 - 27)$$

Finally, a translation is performed with equations **(1 - 28)** and **(1 - 29)** given by:

$$x_i = x_i^* + x_{LE} \quad (1 - 28)$$

$$y_i = y_i^* + y_{LE} \quad (1 - 29)$$

Processor

This part is where the calculations are made, based on the method described. Here is also where one defines if the calculations are to be made with or without ground effect.

Ground effect is simulated with the method of images [16], which consists on placing a mirrored image of the airfoils with the wall as a symmetry axis. As such, the streamline between the airfoils and their respective mirrored images will be a straight line, and hence, in potential theory it can represent a wall. Figure 4 shows this procedure.

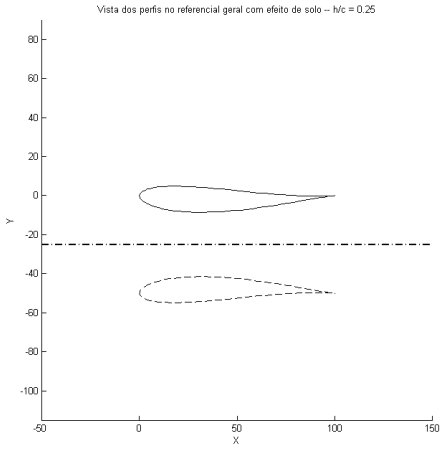

Figure 4 - Method of images

After this process, the calculation proceeds by applying the panel method to all airfoils.

Post-Processor

After the calculation has been made, there are a few ways to see the results. The more obvious ones are visualizing the pressure distributions or by writing the results on a file. Nevertheless one can also view the streamlines or the velocities distribution around the bodies. In order to attain the last options, there is the need to compute the velocities on a grid defined around the airfoils. On the method described earlier, to calculate the velocity on a panel one needs to compute the influence coefficients due to the sources and the vortices on each other panel. Likewise, to compute the influence of all the sources and vortices of a given airfoil on a point of the flow, one needs to apply the panel methods theory. Thus, the tangential and normal influence coefficients are as follow:

$$u_m = V_\infty \cos\alpha + U_{mn} q_n + U_{m,N+1}\gamma \quad (1 - 30)$$

$$v_m = V_\infty \sin\alpha + V_{mn} q_n + V_{m,N+1}\gamma \quad (1 - 31)$$

After this process has been made to every point on the grid and all bodies on the flow have been taken into account, the absolute velocity and the pressure coefficient can be calculated by the following equations:

$$vel_m = \sqrt{{u_m}^2 + {v_m}^2} \quad (1 - 32)$$

$$C_{P_m} = 1 - \left(\frac{vel_m}{V_\infty}\right)^2 \quad (1 - 33)$$

On Figure 5 an example of the visualization of streamlines around two NACA 3312 airfoils is shown:

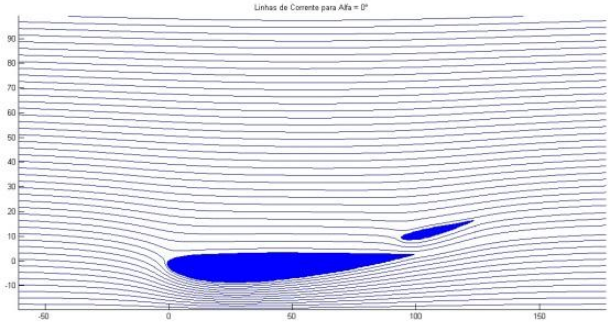

Figure 5 - Streamlines around two NACA 3312

Verification Procedure

On this section the aim is to show that the code is correct. When available, analytical solutions are used to find the numerical error and show that it tends to zero as the number of panels used in the discretization increases. First, the verification procedure was done for single airfoils, and then, for multi-element configurations.

Single-airfoil Verification

To study the numerical error convergence for single-airfoils, there are exact solutions for Kárman-Trefftz and Joukowski airfoils given by conformal mapping. Thus, one can compute the absolute numerical error through the expression:

$$e_{\phi_i} = \phi_i - \phi_{exact} \tag{1 - 34}$$

Where ϕ is the parameter one wishes to analyse. Equation **(1 - 34)** can also be approximated by equation **(1 - 35)** [17], which will help study the convergence of ϕ_i:

$$e_{\phi_i} = e_o + \beta \left(\frac{h_i}{h_1}\right)^p \tag{1 - 35}$$

e_o is the discretization error infinite number of panels, α is a constant to be determined, p is the observed order of asymptotic convergence and $\frac{h_i}{h_1}$ is the grid refinement ratio. e_o should be of the order of the machine precision, and if it is negligible, equation **(1 - 35)** can be written in its logarithmic form:

$$\ln e_{\phi_i} = p \ln\left(\frac{h_i}{h_1}\right) + \ln \beta \tag{1 - 36}$$

Equation **(1 - 36)** can be interpreted as a straight line if p is in the asymptotic region. The goal of this verification procedure is then to find the asymptotic p if that is possible and to show that ϕ_o is negligible.

Results

The results shown here are for a symmetric Kárman-Trefftz airfoil and for a cambered Joukowski airfoil, both with analytical solutions, and then the results for a NACA 5412, where the aim was to show the results for a more common airfoil and without exact solution. The grid refinement parameter is defined as $\frac{h_i}{h_1} = \frac{N_1}{N_i}$, where N_1 is the maximum number of panels used and equals 1280, while N_i varies between 40 and 1280. The parameters analyzed were the lift coefficient computed through the Kutta condition (C_{L_Γ}) and the lift ($C_{L_{int}}$) and drag ($C_{D_{int}}$) coefficients computed through the pressure integration. Hence, the results for the symmetric Kárman-Trefftz can be seen on Figure 6.

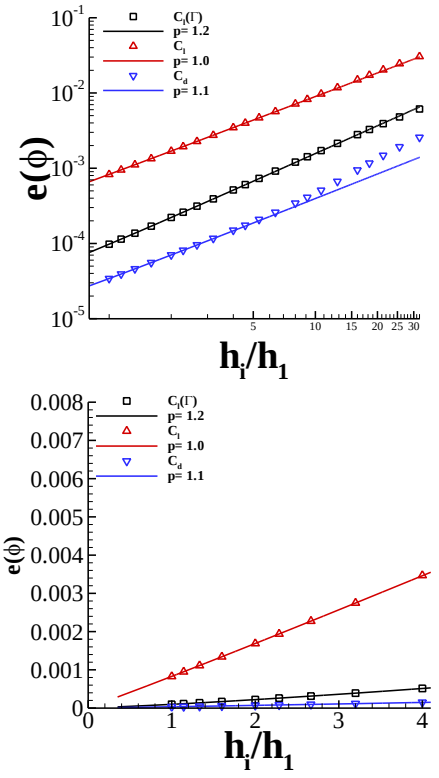

Figure 6 - Results for the symmetric Kárman-Trefftz
a) Logarithmic scale b) Linear scale

It can be seen in plot a) from Figure 6 that all the observed orders of accuracy for the parameters analyzed are within the expected values, i.e., around the order of 1, which is the order of the method used. In plot b), it is shown that all the extrapolation of all the numerical errors tends to zero as the number of panels used increases. As for the cambered Joukowski profile, the results can be seen in Figure 7.

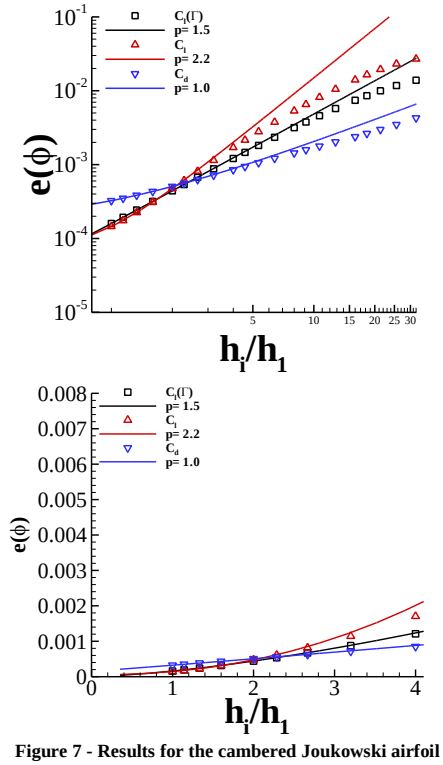

Figure 7 - Results for the cambered Joukowski airfoil
a) Logarithmic scale b) Linear scale

Even though the observed orders of accuracy for C_{L_Γ} and $C_{L_{int}}$ are above the expected (specially $C_{L_{int}}$), one can see by plot b) that the error is very small and that it tends to zero as the number of panels increase. In this case, the data is not in the asymptotic range, i.e. p is still changing.
The results for the NACA 5412 airfoil can be seen in Figure 8.

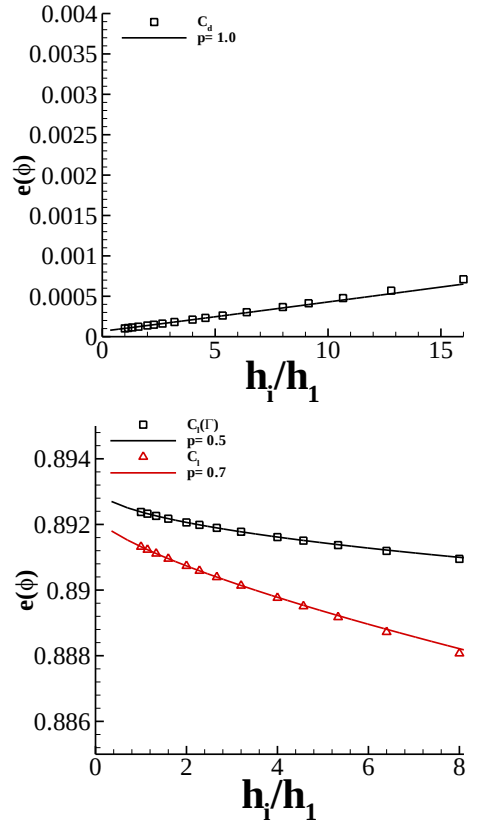

Figure 8 - Results for the NACA 5412
a) Results for Cd b) Results for CL

For this airfoil, the only parameter for which the numerical error can be estimated is the $C_{D_{int}}$, as its value is already an error estimate since in potential theory there should not be any drag. As such, the results for both lift coefficients are the absolute values, and the goal is to show that both converge to a same value. As can be seen in plot a) from Figure 8, the results for $C_{D_{int}}$ show that the numerical error tends to zero as the number of panels tends to infinity ($\frac{h_i}{h_1} = 0$). As for the results for the lift coefficients, it is shown in plot b) that both coefficients converge to a same value as the number of panels used increases, which is within the expected.

It can be concluded that although the numerical error convergence isn't always what should be expected, the results show that there are no major errors in the code and that it produces good results, with the error always decreasing as the number of panels used increases.

Multi-element Verification

In order to make the verification procedure for multi-element configurations, one can no longer count on the analytical solutions available for the single element verification coming from the conformal mapping. Nonetheless, it is still possible to show that the code is behaving as expected and also to estimate the calculation uncertainty. Thus, a plot showing the behaviour of the lift of an airfoil in ground effect as a function of the ground clearance is presented. Also, plots of the lift coefficient as a function the number or panels were used in order to estimate the uncertainty for a certain distance to the wall. The results for a NACA 4412 lift coefficient as function of the distance to the wall (h/c) at $\alpha = 2°$ are shown in Figure 9.

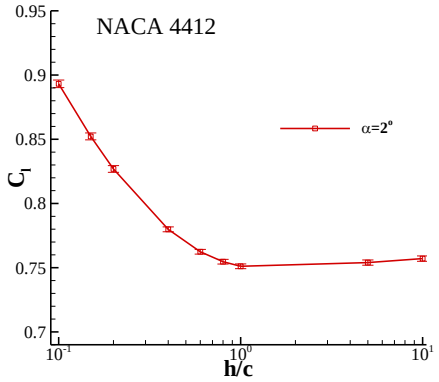

Figure 9 - Lift coefficient vs h/c

It can be seen that the lift is high near the wall and decreases as the distance increases until it reaches a minimum around $\frac{h}{c} = 1$, when it starts increasing again and converges to the value of c_L for the airfoil without ground effect ($C_L = 0.7610$). In order to estimate the uncertainty of the calculation, the airfoils in Table 1 were used:

Airfoil	α	h/c
NACA 0015	0	0.200
NACA 4412	2	0.100
NACA 4412	6	0.500

Table 1 - Characteristics of the profiles used

These airfoils subject to such conditions were used because further on this paper similar situations will be explored, and as such, it is of extreme importance to know how many panels are needed to achieve a certain threshold for the uncertainty. In this case, the aim was to achieve an uncertainty below 1%. For that purpose, calculations were made using panels in the range of 80 and 320. Figure 10 shows the results for the NACA 0015.

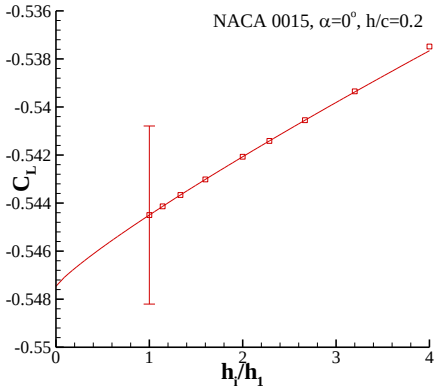

Figure 10 - Results for the NACA 0015, $\alpha = 0°, \frac{h}{c} = 0.2$

The estimated uncertainty for this case was shown to be 0.3707%, well below the 1% threshold, meaning that 320 panels were enough. Figure 11 and Figure 12 show the results for the NACA 4412 airfoil.

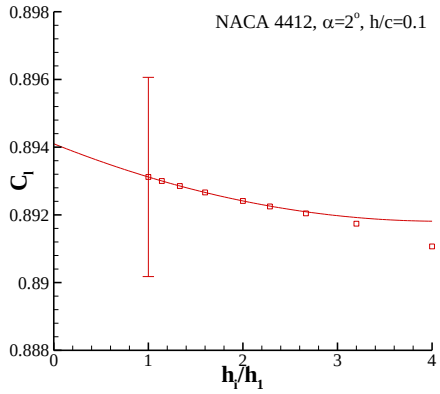

Figure 11 - Results for the NACA 4412, $\alpha = 2°, \frac{h}{c} = 0.1$

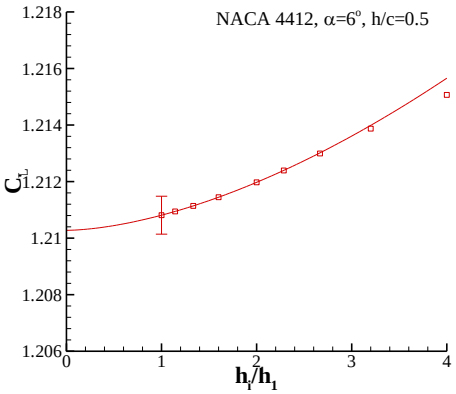

Figure 12 - Results for the NACA 4412, $\alpha = 6°, \frac{h}{c} = 0.5$

The estimated uncertainty for the NACA 4412 was shown to be, respectively for the first and second case, 0.2942% and 0.0671, both also well below the 1% goal, also meaning that the maximum number of panels used was enough.

It can be concluded that the results obtained with the code are the expected and that calculations with 320 panels are enough to obtain a numerical uncertainty lower than 1% for ground effect applications. Nevertheless, in all the results obtained it is always shown an uncertainty bar in order to prove that the calculation uncertainty is smaller than variations due to changing calculation parameters.

Applications Examples

The aim of this section is to demonstrate some possible situations to which the code developed can be used and also to show that the results obtained are similar to results found in the literature obtained through experimental procedures or by CFD codes. On a first approach, configurations with airfoils in ground effect will be explored, where results will be compared. On a second approach, a rotor of a vertical axis wind turbine will be investigated, where the aim was to study several configurations for a two airfoil rotor in order to reduce the minimum pressure coefficient at high angles of attack, a situation that is common in this kind of turbines.

Airfoils in Ground Effect

A typical application for this kind of methods is the ground effect, which is very easy to reproduce through the method of images. Generally speaking, the lift coefficient of an airfoil will increase when it is close to the ground [18], although there are some exceptions, which are shown in the following examples. The distance to the ground h will be defined as one of the possibilities in Figure 13.

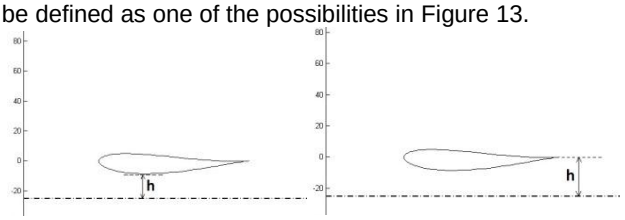

Figure 13 - Possible definitions of h.
a) Ground clearance b) Distance to the trailing edge

In all the following examples the definition of h will be defined beforehand.

NACA 0015 Airfoil

In this analysis a NACA 0015 was subject to ground effect at a 0° angle of attack. The results to be compared were obtained with an inviscid 2nd order panel method obtained by Caresse, R., available in [19]. The distance to the ground is that of image b) in Figure 13. Both results can be seen in Figure 14.

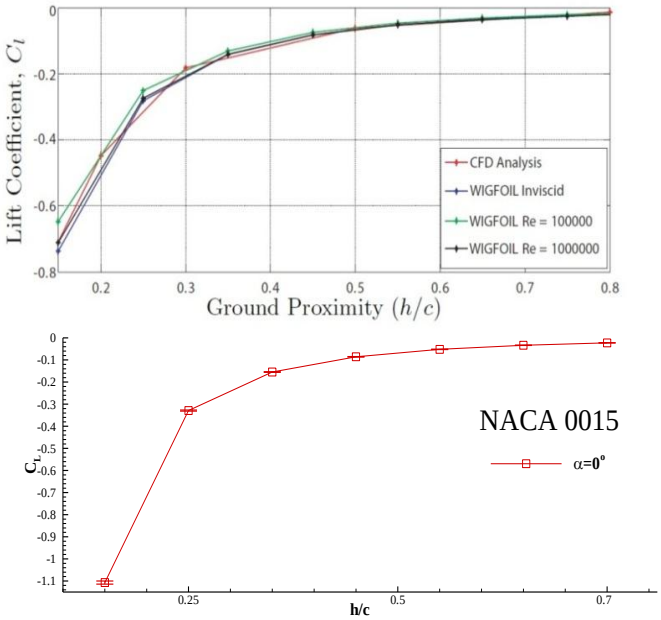

Figure 14 - Comparison of results of a NACA 0015 in ground effect
a) Fig. 5 from [19]. b) Results obtained with the program.

It can be seen that both trends of the lift coefficient are very similar, showing that comparisons with other inviscid methods produce the same type of results.

NACA 4412 Airfoil

The NACA 4412 was first analyzed at the same ground clearances and same angles of attack as those used in a CFD calculation performed by Rong, W. and presented in [18]. The ground clearance definition is that of image a) in Figure 13. Both results are shown in Figure 15.

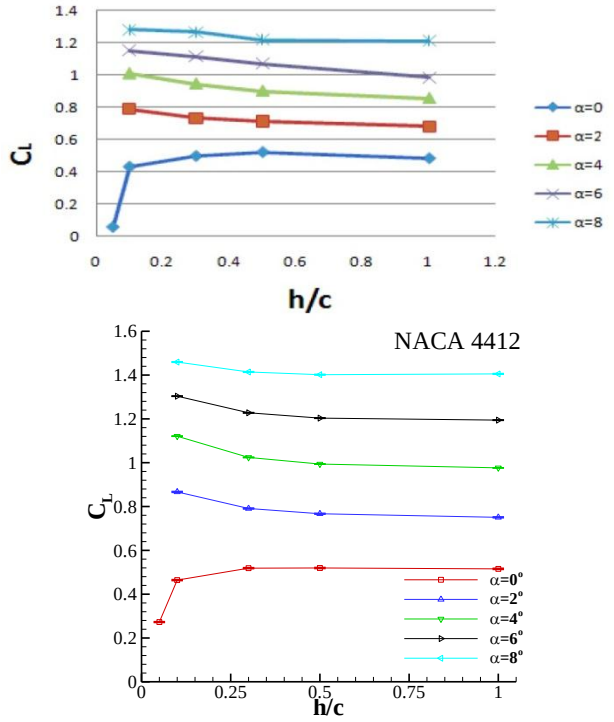

Figure 15 - Results for the NACA 4412.
a) Fig. 6 of [18]. b) Results obtained with the program.

By comparing both plots, one can conclude that for every angle of attack the trends are the same. Only for $\alpha = 0°$ the lift coefficient decreases when the distance to the ground also decreases. For all the other angles of attack the lift increases as ground clearance decreases. The values for the lift obtained by the code are always somewhat overestimated when compared to those in plot a), but that is due to the fact that this method is inviscid as opposed to the CFD results which are not.

Other results obtained by Hsiun, C. [20] were analyzed for the NACA 4412. Both results can be seen in Figure 16 and Figure 17.

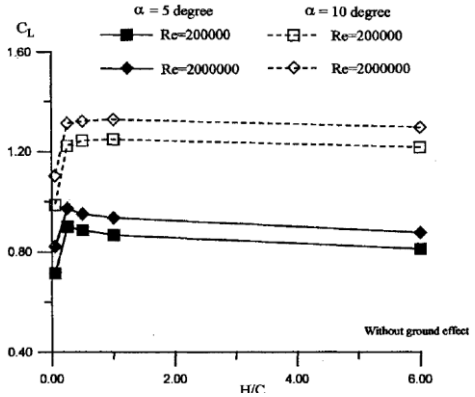

Figure 16 - Results for the NACA 4412.
a) Fig. 13 of [20].

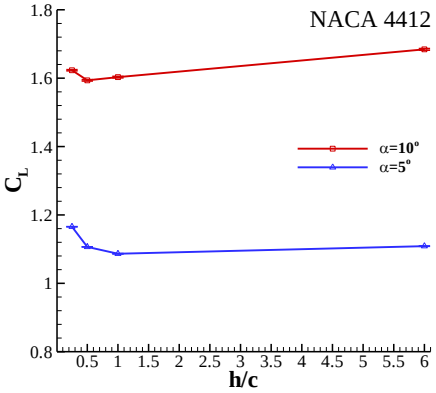

Figure 17 - Results for the NACA 4412.
b) Results obtained with the program.

Being this a potential flow method, the Reynolds number is infinite, and hence, the results should be compared with the higher Reynolds number results in a). Although it seems that there isn't much correlation between the results, the results from $\frac{h}{c} = 1$ until $\frac{h}{c} = 0.25$ are similar in both plots for $\alpha = 5°$. The same is not true to $\alpha = 10°$ due to the very high viscous effects at this angle. At $\alpha = 10°$, the trend is for the lift to increase near the wall at a bigger Reynolds number, leading one to think that the trend would be for the lift to increase even more near the wall at a higher Reynolds number.

Figure 18 shows the pressure distribution for the NACA 4412 at $\alpha = 5°$ available in [20] and the corresponding pressure distributions obtained with the code developed.

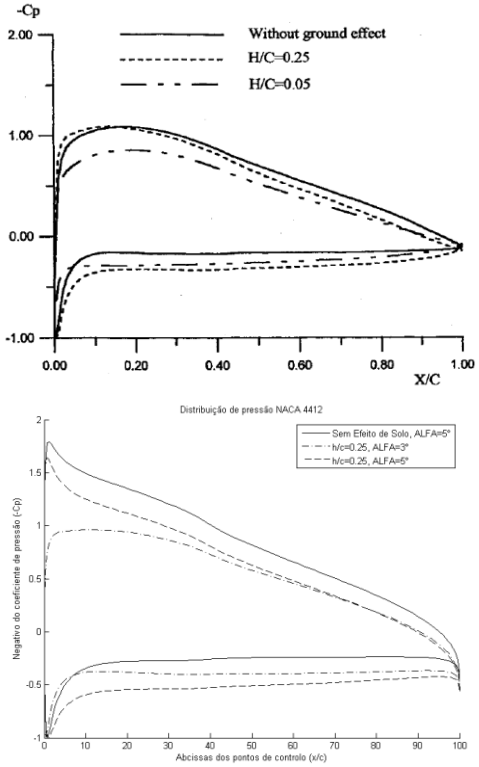

Figure 18 – Pressure distributions for the NACA 4412
a) Fig. 14 from [20]. b) Results obtained with the program

Relating to plot a) from Figure 18, the results that were analyzed were that of the calculation without ground effect and that with $\frac{h}{c} = 0.25$. Observing the corresponding

results in plot b), calculations were made at $\alpha = 5°$ and $\alpha = 3°$. The reason why the pressure distribution at $\alpha = 3°$ was also calculated is because, as the effect of the boundary layer is to reduce the effective angle of attack, the equivalent angle of attack for the same lift coefficient was found to be $3°$ based on fig. 3 from [20]. The minimum pressure at $\alpha = 5°$ both for $\frac{h}{c} = 0.25$ and without ground effect is much more prominent than the corresponding ones found in plot a). Nevertheless, if one compare the results for $\frac{h}{c} = 0.25$ at $\alpha = 3°$, the results are much more similar, as would be expected.

NACA 0012 Airfoil

Following the same process done for the previous airfoils, results for the NACA 0012 also obtained by Caresse, R. in [19] were compared to those obtained through the developed code. The definition of h/c used was that of image b) in Figure 13. The results are shown in Figure 19.

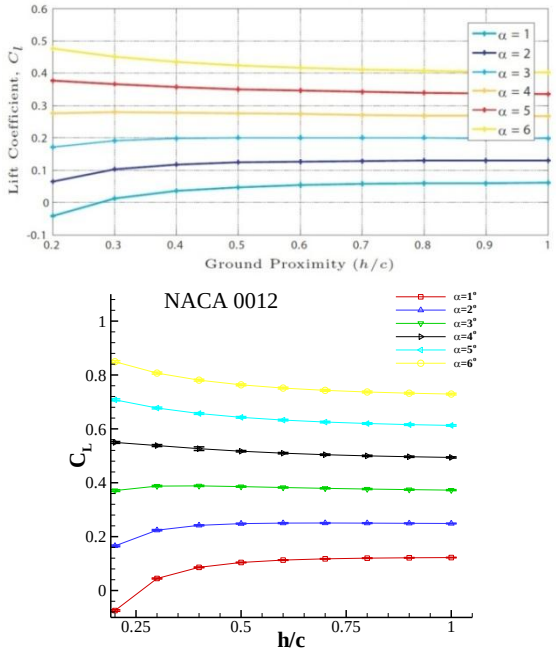

Figure 19 - Results for the NACA 0012.
a) Fig. 10 from [19]. b) Results obtained with the program.

Once more it is shown that the trends of the lift coefficient are the same in both plots. Although the results of b) are again somewhat overestimated, the goal of this comparison was to show that the trends are the same, a goal that was achieved.

Inverted Tyrrell026 Airfoil

In order to bring a little variety to these applications, the next results were performed for an inverted airfoil used in the front wing of a Formula One car. This airfoil was analyzed by Genua, E. [21] and by Zerihan, J. [22], though the results shown here are from [21]. The angle of attack of the calculations was at $\alpha = 3.6°$, a rotation that brought the leading edge closer to the ground. The definition of h/c used was that of image a) in Figure 13.

In Figure 20 the results are shown both for those available in [21] and those obtained with the developed code. The lift coefficient presented is the absolute value, since being an inverted airfoil, the lift points downwards.

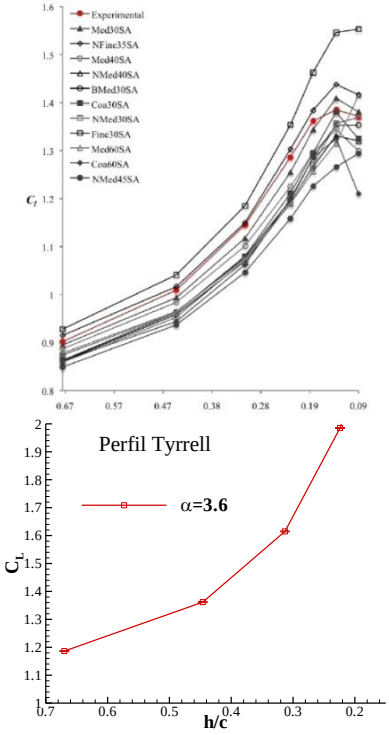

Figure 20 - Results for the Tyrrell026.
a) Fig. 9 of [21]. b) Results obtained with the program.

The trend of the downforce obtained in b) is very similar to the experimental one (red line in a)) until $h/c = 0.18$, when the experimental results drop abruptly due to the occurrence of flow separation near the trailing edge.

Double Rotor of a Vertical Axis Turbine

In this section the goal was to demonstrate that the code developed can be used to search for an optimum configuration in order to reduce the suction peak for a vertical axis turbine rotor. The configurations tested are in Table 2 and Figure 21. The colors correspond to the different configurations used, with the black airfoil being common to all configurations. The airfoils used were the NACA 0015.

Configuration nr.	Airfoil 1		Airfoil 2		Color
	LE	TE	LE	TE	
1	(0,0)	(100,0)	(0,30)	(100,30)	Blue
2	(0,0)	(100,0)	(0,45)	(100,45)	Cyan
3	(0,0)	(100,0)	(0,115)	(100,115)	Red
4	(0,0)	(100,0)	(50,30)	(150,30)	Green
5	(0,0)	(100,0)	(100,30)	(200,30)	Black

Table 2 - Configurations tested

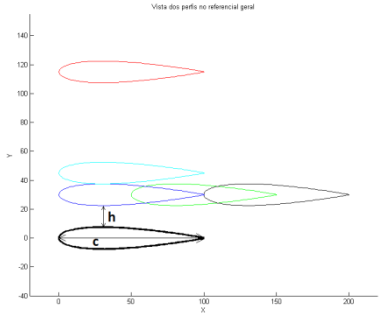

Figure 21 - Configurations tested

Figure 22 shows the minimum pressure plotted as a function of the total lift coefficient generated by both airfoils.

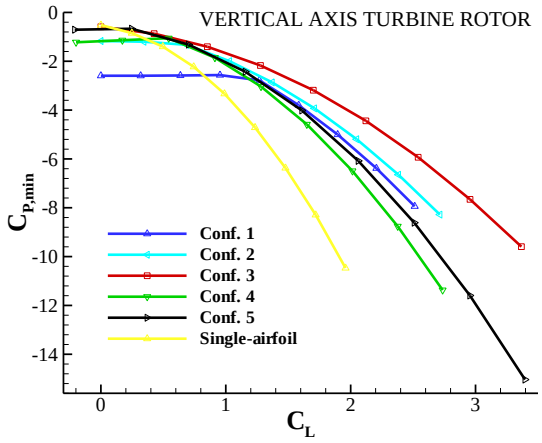

Figure 22 - Cp,min vs CL

This plot could be used to decide which configurations would best suit the predefined specifications, after which other CFD codes could be used to further investigate the selected configurations.

Conclusions

A versatile MATLAB code for solving the potential flow around multi-element bodies based on a 2D panel method was developed. The order of convergence was found for single-element airfoils and the uncertainty was computed for multi-element configurations. By comparing results obtained through the developed code with those found in the literature, it was shown that the program produces similar trends for the lift coefficient and pressure distribution, even if the absolute values are usually overestimated due to the fact that viscous effects are not taken into account. It can be concluded that the code can be used in several applications where the expected results are the trends of variation of the aerodynamic coefficients instead of the exact values, the latter situation being one in which CFD codes are more assertive. It can be used in optimization procedures due to the reduced computation time, allowing it to be run for example in genetic algorithms.

References

[1] Hess, J.L. *Review of the Source Panel Technique for Flow Computation.* Atlanta, Georgia, Douglas Paper, 1986.

[2] Sun, S., Thannipat, P. and Winarto, H. *Airfoil Shape Optimization for a Formula One Car Front Wing Using Multi-Objective Genetic Algorithm.* American Institute of Aeronautics and Astronautics.

[3] Wickramasinghe, U., Carrese, R and Li, Xiaodong. *Designing Airfoils using a Reference Point based Evolutionary Many-objective Particle Swarm Optimization Algorithm.* Barcelona, Spain, World Congress on Computational Intelligence, July, 18-23, 2010.

[4] Katz, J. *Aerodynamic Model for Wing-Generated Down Force on Open-Wheel-Racing-Car Configurations.* SAE Publication 860218, 1986.

[5] Katz, J. *Calculation of the Aerodynamic Forces on Automotive Lifting Surfaces.* ASME J. Fluids Eng., 107, pp. 438–443, 1985.

[6] Katz, J. *Considerations Pertinent to Race-Car Wing Design.* Loughborough University Conference on Vehicle Aerodynamics, pp. 23.1–23.7, 1994.

[7] Katz, J. *High-Lift Wing Design for Race-Car Applications.* SAE Publication 951976, 1995.

[8] Knowles, K., Donahue, D. T. and V., Finnis M. *A Study of Wings in Ground Effect.* Loughborough University Conference on Vehicle Aerodynamics, Vol. 22, pp. 1–13, 1994.

[9] Eça, L. and Falcão de Campos, J. *Analysis of Two-Dimensional Foils Using a Viscous-Inviscid Interaction Method.* Int. Shipbuilding Progress, Vol. 40, no. 422, pp.137-163, 1993. ISSN 0020-868X.

[10] Hess, J.L. and Smith, A.M.O. *Calculation of Potential Flow About Arbitrary Bodies.* New York, Pegamon Presser, 1966.

[11] Katz, J. and Plotkin, A. *Low-Speed Aerodynamics.* Singapore : McGraw Hill, 1991. ISBN 0-07-050446-6.

[12] Mason, B. *Applied Computational Aerodynamics.* http://www.dept.aoe.vt.edu/~mason/Mason_f/CAtxtTop.html.

[13] Moran, J. *An Introduction to Theoretical and Computational Aerodynamics.* Mineola, New York, Dover Publications, 1984. ISBN 0-486-42879.

[14] Brederode, Vasco de. *Fundamentos de Aerodinâmica Incompressível.* Lisboa, Edição de Autor, 1997.

[15] Pina, Heitor. *Textos de Matemática Computacional.* Faculdade de Engenharia da Universidade do Porto, 2008.

[16] Falcão, António. *Mecânica dos Fluidos II: Escoamento de Fluidos Perfeitos.* AEIST, 2005.

[17] Eça, L., Vaz, G. and Falcão de Campos, J. *Verification Study of Low and Higher-Order Potential Based Panel Methods for 2D Foils.* American Institute of Aeronautics and Astronautics, no. 2002-3112, 2002.

[18] Rong, W., Feng, Liang and L., Wenxiang. *Computational Analysis on Aerodynamics of The Airfoil in Ground Effect.* Xiamen, China, International Conference on Computer Science and Electronics Engineering, 2012.

[19] Carrese, R. and Winarto, H. *Parametric Study of Airfoil Proximity to the ground.* Bundoora, Australia, American Institute of Aeronautics and Astronautics.

[20] Hsiun, C. and Chen, C. *Aerodynamic Characteristics of a Two-Dimensional Airfoil with Ground Effect.* Journal of Aircraft, Vol. 3, No. 2, 1996.

[21] Genua, E. *A CFD Investigation into Ground Effect Aerodynamics.* Master Thesis, Delft University of Technology, 2009.

[22] Zerihan, J. and Zhang, X. *Aerodynamics of a Single-Element in Ground Effect.* Journal of Aircraft, Vol. 37, Nº 6,2000, pp. 1058-1064.